Accepted Manuscript

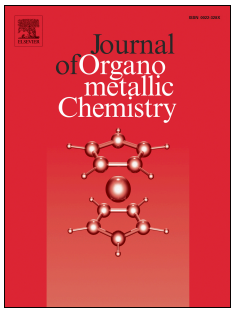

Synthesis, antiproliferative activity and apoptosis-promoting effects of arene ruthenium(II) complexes with N, O chelating ligands

Nanjan Mohan, Mohamed Kasim Mohamed Subarkhan, Rengan Ramesh

PII: S0022-328X(18)30022-6

DOI: 10.1016/j.jorganchem.2018.01.022

Reference: JOM 20260

To appear in: *Journal of Organometallic Chemistry*

Received Date: 31 October 2017

Revised Date: 8 January 2018

Accepted Date: 16 January 2018

Please cite this article as: N. Mohan, M.K. Mohamed Subarkhan, R. Ramesh, Synthesis, antiproliferative activity and apoptosis-promoting effects of arene ruthenium(II) complexes with N, O chelating ligands, *Journal of Organometallic Chemistry* (2018), doi: 10.1016/j.jorganchem.2018.01.022.

Synthesis, antiproliferative activity and apoptosis-promoting effects of arene ruthenium(II) complexes with N, O chelating ligands

Nanjan Mohan, Mohamed Kasim Mohamed Subarkhan and Rengan Ramesh*

Centre for Organometallic Chemistry, School of Chemistry, Bharathidasan University, Tiruchirappalli 620 024, Tamil Nadu, India

A B S T R A C T

New half sandwich arene ruthenium(II) complexes of the type [Ru(arene)Cl(L)] (where arene= benzene and *p*-cymene, L = thiophene benzhydrazone ligands) have been synthesized from the reactions of the neutral precursor [Ru(arene) (μ-Cl) Cl]$_2$ and the corresponding benzhydrazone ligand. All the complexes were completely characterized by elemental analysis and additionally by IR, UV-Vis, ^{1}H NMR and ESI-MS spectroscopic methods. The solid state structures of the complexes 6 and 7 were determined by single-crystal X-ray diffraction analysis, which exhibit typical pseudo-octahedral geometry around the metal center. The antiproliferative activity of the complexes was evaluated on cancerous (HeLa, MDA-MB-231, and Hep G2) and noncancerous (NIH3T3) cell lines. In general, complexes containing electron releasing OCH_3 substituent have potential anticancer activity than those incorporating H, Cl and Br substituents. Moreover, the *p*-cymene complexes show more cytotoxicity than benzene derivatives, suggesting that the substituent at arene plays a vital role in the biological activity of the compounds. Further, an apoptotic mechanism of cell death in MDA-MB-231 was confirmed by AO-EB, Hoechst 33258 staining and annexin-V/PI double-staining techniques. In addition, the extent of DNA fragmentation in cancer cells was studied by comet assay.

Keywords:

Benzhydrazone; η^6-arene ruthenium(II) complex; Crystal structure; Cytotoxicity; Apoptosis

* Corresponding author. Tel.: +91 431 2407053; fax: +91 431 2407045.

E-mail address: ramesh_bdu@yahoo.com, rramesh@bdu.ac.in (R. Ramesh).

1. Introduction

Although platinum-based drugs cisplatin, carboplatin and oxaliplatin have been widely used for anticancer agents for the past few decades, the problems of high toxicity, platinum resistance and undesirable side-effects are appealing the search for different transition metal anticancer drugs**.** It is to note that ruthenium-complexes have attracted significant attention among the other various metal complexes for their potential anticancer activity. In this regard ruthenium complexes exhibit evidence of low toxicity compared to traditional cisplatin agents. The ruthenium(III) complexes particularly [imiH_2] [trans-Ru(N-imiH)(S-dmso)Cl4] NAMI-A and [indH2][trans-Ru(N-indH)2Cl4] KP1019 [1,2] and its sodium analogue Na[trans-Ru(N-indH)2Cl4] (NKP-1339 or IT-139) are the most promising ruthenium complexes reaching clinical trials [3]. Notably, the activation method depends on the redox potential of the Ru(III)/Ru(II) oxidation states, which in turn strongly depends on the ligands coordinated to the metal centre. The activation by reduction results in a reactive ruthenium(II) complex, which can react with numerous biomolecules [4-7].

Particular attention has been paid to half sandwich arene ruthenium complexes because of the π-ligated arene which confers great stability to Ru in the +2 oxidation state and influences the hydrophobicity and interaction with biomolecules [8-10]. Substitutions at arene moiety and variations in the chelating ligands will be able to fine tune their biological properties [11]. Tocher et al. have reported that cytotoxicity was enhanced by coordinating the antibacterial agent metronidazole [1-β-(hydroxyethyl)-2-methyl-5-nitro-imidazole] to a benzene ruthenium dichloro fragment [12]. At first, the prototype arene ruthenium(II) complexes [(p-Me$C_6H_4Pr^i$)$RuCl_2$(P-pta)] (pta = 1,3,5-triaza- 7-phospha-tricyclo-[3.3.1.1]decane), termed RAPTA-C [13] which displays pH dependent DNA damage due to the hypoxic (low pH) nature of cancer cells, and [(C_6H_5Ph)RuCl(N,N-en)][PF6] (en = 1,2-ethylenediamine) exhibits selective binding to guanine bases on DNA, forming monofunctional adducts [14] , though many various categories have since been reported [15].

Hydrazones are versatile ligands with fascinating ligation properties with many transition metals. Moreover, these ligands represent an important class of compounds for new drug development because hydrazone moiety was selected for its high stability at physiological pH and lability under strongly acidic and basic conditions as incontestable by drug delivery agents in tumor targeting. Thus, all the hydrazones possess the azomethine (-CONHN=CH-) group have been revealed to exhibit antiproliferative activities and act as cytotoxic agents

with the ability to stop cell progression in cancerous cells through different mechanisms [16]. Aroylhydrazones are magnificent multidentate ligands for transition metals. They have been exhibit to reveal a variety of biological e.g. antiamoebic activity [17] and DNA synthesis inhibition or antiproliferative behaviour [18-20]. Herein, we present a systematic investigation of half-sandwich Ru(II) complexes bearing benzhydrazone ligands (Fig. 1) with respect to their antiproliferative activity on human cancer cells.

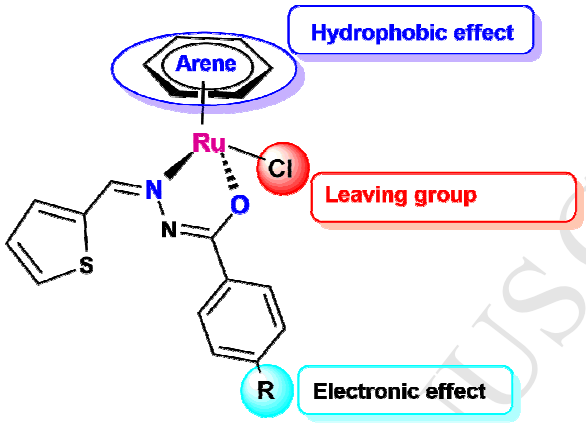

Fig. 1 Design of arene ruthenium(II) benzhydrazone complexes.

2. Results and discussion

The benzhydrazones were obtained by condensation of equimolar amounts of thiophene-2-carboxyaldehyde and substituted benzhydrazide [21]. The arene complexes of the type [Ru(arene)Cl(L)] (arene= benzene and *p*-cymene and L = thiophene benzhydrazone ligands) (Scheme 1) have been synthesised from the reactions of the ligands and ruthenium arene dimers [Ru(arene) (μ-Cl)Cl]$_2$ in a 2 : 1 molar ratio in benzene for 5h at reflux temperature in the presence of triethylamine as a base. The isolated complexes were yellow, brown in colour, air stable solids, partially soluble in water and completely soluble in polar organic solvents like methanol, ethanol, acetone, chloroform, dichloromethane, acetonitrile, dimethylformamide and dimethylsulfoxide. The elemental analysis of all the ruthenium(II) complexes are in good agreement with the molecular formula of the proposed structure.

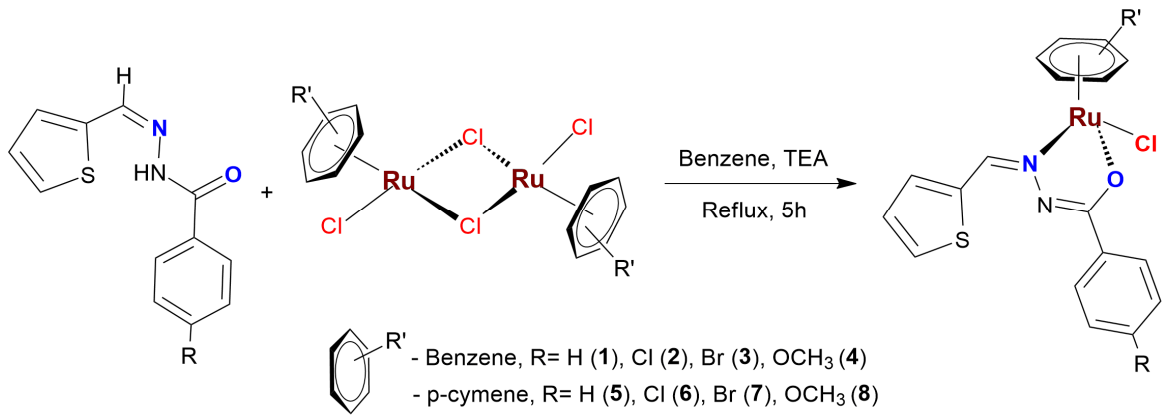

Scheme 1. Synthesis of arene ruthenium(II) benzhydrazone complexes.

FT-IR spectra of the ligands and the complexes (1-8) furnished significant information about coordination of the ligand to metal. A medium to strong band in the range 3191-3280 cm^{-1} was assigned to the N-H functional group of the ligand. The ligands also exhibit absorptions due to $\nu_{C=N}$ and $\nu_{C=O}$ within the range 1632-1649 cm^{-1}. Upon complexation the bands associated with ν_{N-H} and $\nu_{C=O}$ stretching vibrations are disappeared and indicating that the ligands undergo tautomerization and consequent coordination of the imidolate oxygen. The appearance of new bands in the range 1259-1272 and 1594-1620 cm^{-1} attributed to the C–O and C=N–N=C fragments which give further support for the coordination of the ligand. Hence, the coordination through imine nitrogen and the imidolate oxygen of the ligand to ruthenium was confirmed by IR spectra of all the complexes [22]. All the complexes show three bands in the region 234-366 nm in acetonitrile at room temperature. Bands due to ligand-centered (LC) transitions are appeared around 234-304 nm and have been designated as π–π* and n–π* transitions. The lowest energy bands that appeared in the region 360-366 nm were attributed to the charge transfer due to metal to ligand transitions [23]. The pattern of the electronic spectra of all the complexes is very similar to other previously reported octahedral complexes. Fig. S1-S8 (ESI†).

The binding of the benzhydrazone ligand to the ruthenium(II) ion is further verified by NMR spectra of the complexes. All the complexes show multiplets in the region δ 6.7- 8.1 ppm and have been assigned to the aromatic protons of benzhydrazone ligands. A sharp singlet in the region δ 8.8-8.9 ppm is assigned to azomethine proton which shifted to downfield on comparison with those of the free ligands, indicating deshielding of the azomethine proton upon coordination to ruthenium. In addition, the absence NH proton of the

free ligands in all the complexes confirmed the coordination to Ru(II) ion via imidolate oxygen. An upfield shift of η^6-C_6H_6 protons of 1-4 has been observed in the region of δ 5.5 ppm. Two sets of doublets have been observed in the region δ 1.0-1.3 ppm for the methyl protons of isopropyl group in *p*-cymene moiety. The methine proton of the isopropyl group appears as a septet in the range of δ 2.5-2.6 ppm. Further, a singlet at δ 2.2 ppm is attributed to the methyl protons of the *p*-cymene moiety. Moreover, four sets of doublets in the range of δ 4.6-5.3 ppm were assigned to the aromatic protons of the *p*-cymene ligand. In addition, for complexes 4 and 8 the methoxy signals of the benzhydrazone ring were observed as a singlet at δ 3.8 and δ 3.7 ppm. Thus the ^{1}H NMR spectra of all the complexes confirm the coordination mode of the benzhydrazone ligand to the ruthenium(II) ion through the azomethine nitrogen and the imidolate oxygen Fig. S9-S16 (ESI†).

2.1 Crystal structures

Single crystal X-ray diffraction analysis of the complexes 6 and 7 were grown from CH_2Cl_2/ Pet .ether by slow evaporation method. The ORTEP diagrams for the two structures are shown in Fig. 2, crystallographic data and selected bond parameters are listed in Table 1 and 2. Both complexes 6 and 7 crystallize in the monoclinic space group $P2_1/c$. In the complex 6, the (η^6-*p*-cymene) ligand occupying three coordination sites in η^6-fasion and the remaining coordination sites are occupied by N, O donor atoms from chelating ligand and one chloride. Thus the crystallographic structure of complex confirms pseudo octahedral geometry around the ruthenium metal [24]. The Ru-N, Ru-O and Ru–Cl bond lengths are 2.107(4), 2.056(3) and 2.398(13) Å, respectively. The Ru-C (p-cymene) bond lengths ranging from 2.157-2.221 Å and p-cymene ring C-C bond lengths ranging from 1.398-1.432 Å. Bond angles of $86.18(11)^0$, $85.73(11)^0$ and $76.23(13)^0$ are observed for Cl-Ru-O, Cl-Ru-N, and N-Ru-O respectively. A similar structural feature has been found in complex 7 with marginal changes in bond lengths and bond angles.

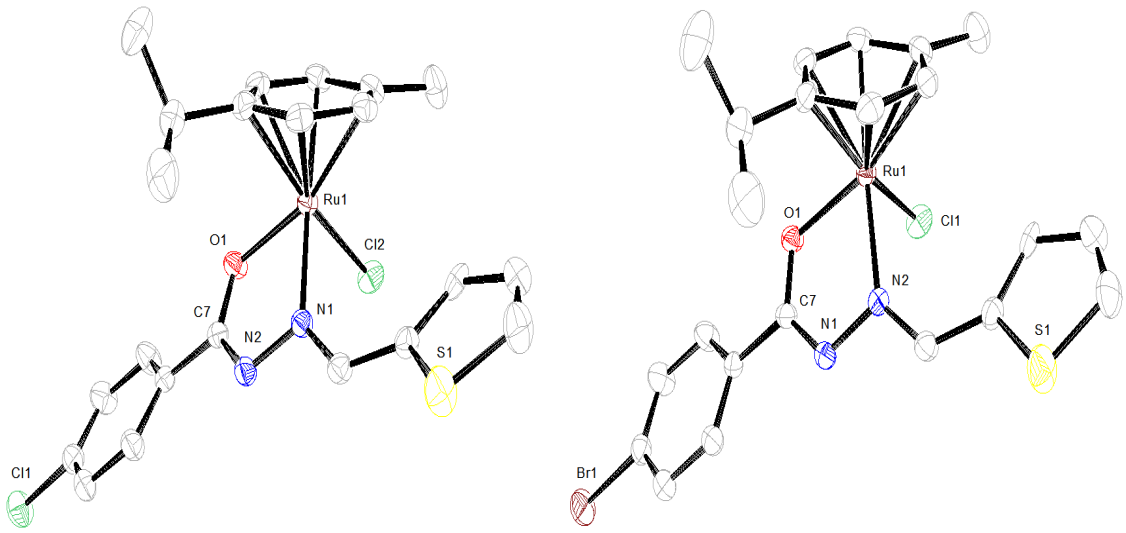

Fig. 2 Molecular structures of complexes 6 and 7; thermal ellipsoids are drawn at the 30% probability level. All hydrogen atoms were omitted for clarity.

Table 1 Selected Bond Lengths (Å) and Angles (deg) for the Complexes **6** and **7**

6		**7**	
Bond lengths (Å)			
N(1)-N(2)	1.413(5)	N(1)-N(2)	1.410(6)
N(1)-Ru(1)	2.107(4)	N(2)-Ru(1)	2.107(4)
O(1)-Ru(1)	2.056(3)	O(1)-Ru(1)	2.053(3)
Cl(1)-Ru(1)	2.398(13)	Cl(1)-Ru(1)	2.400(15)
C(7)-O(1)	1.305(5)	C(7)-O(1)	1.300(6)
C(7)-N(2)	1.299(6)	C(7)-N(1)	1.300(6)
C(8)-N(1)	1.288(6)	C(8)-N(2)	1.296(6)
Bond angles (^{0})			
N(2)-N(1)-Ru(1)	113.5(3)	N(1)-N(2)-Ru(1)	113.7(3)
C(7)-N(2)-N(1)	110.9(4)	C(7)-N(1)-N(2)	110.9(4)
C(7)-O(1)-Ru(1)	112.6(3)	C(7)-O(1)-Ru(1)	112.9(3)
O(1)-Ru(1)-N(1)	76.23(13)	O(1)-Ru(1)-N(2)	76.09(15)
O(1)-Ru(1)-Cl(2)	86.18(11)	O(1)-Ru(1)-Cl(1)	85.76(12)
N(1)-Ru(1)-Cl(2)	85.73(11)	N(2)-Ru(1)-Cl(1)	85.80(12)

ESD in parenthesis.

Table 2 Crystal data and structure refinement for complexes **6** and **7**

Compound	**6**	**7**
Empirical formula	$C_{22}H_{22}Cl_2N_2O_2RuS$	$C_{22}H_{22}BrClN_2O_2RuS$
Formula weight	550.45	594.91
Temperature	296(2) K	296(2) K
Wavelength	0.71073Å	0.71073 Å
Crystal system	Monoclinic	Monoclinic
Space group	P21/c	P21/c
Unit cell dimensions	*a = 13.9604(5)Å alpha = 90 deg.*	a = 13.9337(6)Å alpha = 90 deg.
	b = 17.0717(6) Å beta = 100.359(2) deg.	b = 17.2743(8)Å beta = 101.267(2) deg.
	c = 10.2549(4)Å gamma = 90 deg.	c = 10.3593(4) Å gamma = 90 deg.
Volume	2404.19(15) $Å^3$	2445.38(18)$Å^3$
Z, Calculated density	4, 1.521Mg/m^3	4, 1.616 Mg/m^3
Absorption coefficient	0.981 mm^{-1}	2.490 mm^{-1}
F(000)	1112	1184
Crystal size	0.30 x 0.30 x 0.25 mm	0.35 x 0.30 x 0.30mm
Theta range for data collection	1.48 to 28.35 deg.	1.49 to 28.32 deg.
Limiting indices	$-18 \le h \le 12$, $-22 \le k \le 22$, $-13 \le l \le 13$	$-17 \le h \le 18$, $-19 \le k \le 22$, $-13 \le l \le 10$
Reflections collected / unique	19987 / 5955 [R(int) = 0.0291]	19409 / 5975 [R(int) = 0.0324]
Completeness to theta = 28.44	99.2 %	98.3 %
Absorption correction	Semi-empirical from equivalents	Semi-empirical from equivalents
Max. and min. transmission	0.7915 and 0.7573	0.5221 and 0.4761
Refinement method	Full-matrix least-squares on F^2	Full-matrix least-squares on F^2
Data / restraints / parameters	5955 / 0 / 271	5975 / 0 / 271
Goodness-of-fit on F^2	1.124	1.088
Final R indices [I>2sigma(I)]	R1 = 0.0505, wR2 = 0.1655	R1 = 0.0505, wR2 = 0.1631
R indices (all data)	R1 = 0.0679, wR2 = 0.1888	R1 = 0.0765, wR2 = 0.1816
Largest diff. peak and hole	2.583 and -0.677 e.$Å^{-3}$	2.342 and -0.753 e.$Å^{-3}$

2.2 Stability of the complexes (time-dependent spectra)

Stability of compounds in solution is an essential requirement for drug candidates. The stability of complexes (1-8) in a solution of buffer-DMSO was explored using UV-Vis spectroscopy Fig.S9-S16 (ESI†). The spectra did not exhibit any noticeable changes during a period of 24 hour indicate the stability of the complexes. Further, ESI-MS spectral studies of the complexes confirm the composition. All the complexes showed the characteristic peaks at m/z 410.00 (1, M-Cl^+), 444.96 (2, M−Cl^+), 486.89 (3, M – Cl^+), 439.00 (4, M−Cl^+), 465.05 (5, M−Cl^+), 499.06 (6, M−Cl^+), 544.96 (7, M−Cl^+), and 495.06 (8, M−Cl^+) Fig. S25-S32 (ESI†). The results strongly indicate that the chlorine atom in these complexes is highly labile and the resulting species easily interacts with biomolecules [25].

2.3 Partition Coefficient Determination

Hydrophobicity is the basic physiochemical parameters in the design of drugs and their biological processes [26] and is determined by the n-octanol/water partition coefficient (P) method [27]. Moreover, Log P, were measured to explain the permeability of complexes (1-8) through a biological system [28] based on solubility of a given compound in a two-phase system [29]. The log P results are presented in Table S1(ESI†). The partition coefficient values (log P) of the complexes suggested that hydrophobicity can be arranged in the order 8 > 4 > 6 > 7 > 5 > 2 > 3 > 1.

2.4 Cytotoxicity studies

The cytotoxicities of the metallic precursors, ligands and complexes were determined by spectrofluorimetric MTT assay. The plot of percentage of cell death versus concentration is illustrated in Fig. S33&34 (ESI†). The cytotoxicity of the complexes was expressed by IC_{50} values and are reported in Table 3. It is to be noted that the precursor and the ligand did not show any inhibition even up to 100 µM and the observed cytotoxicity of the complexes is mainly due to chelation of the ligand to ruthenium. The *in vitro* anticancer activity of the Ru-arene complexes 1-8 towards several human cancer cell lines (HeLa, MDA-MB-231, and Hep G2) and a normal human cell line (NIH3T3) were determined after 24 h inhibition and cisplatin was used as a positive control. Based on IC_{50} values obtained, *in vitro* anticancer activity of the complexes follows the order: 8>4>6>7>5cisplatin = 1>2>3. These results are also consistent with hydrophobicity of the complexes [30]. Complexes 1–8 show markedly increased cytotoxic potencies compared with the respective hydrazone

ligands. A comparison of the IC_{50} values of these complexes against MDA-MB-231cells indicates that complexes 4 and 8 exhibits comparatively better than the other complexes under same experimental conditions. The complexes containing methoxy substituent exhibit higher hydrophobicity and enables permeation of complexes across cell membranes [31]. Further, the arene group plays significant role in the antiproliferative activity of these complexes. In general *p*-cymene complexes show higher cell killing activities which may be due to the higher hydrophobic interactions between p-cymene complexes and the biomolecules. Thus, the *in vitro* anticancer activity of the complex towards NIH-3T3 (non-cancerous cells) was determined to be above 221 µM, confirms that these complexes are specific for cancer cells.

Table 3 The cytotoxic activity of arene ruthenium(II) benzhydrazone complexes after 24 h exposure

Complexes	[a]IC_{50} values (μM)			
	HeLa	MDA-MB-231	Hep G2	NIH3T3
L1	>100	>100	>100	>100
L2	>100	>100	>100	>100
L3	>100	>100	>100	>100
L4	>100	>100	>100	>100
$[(benzene)RuCl_2]_2$	>100	>100	>100	>100
$[(p\text{-}Cymene)RuCl_2]_2$	>100	>100	>100	>100
1	32.5 ± 0.3	19.6 ± 0.3	26.9 ± 0.1	223.7 ± 0.8
2	28.6 ± 0.4	18.7 ± 0.2	21.3 ± 0.5	232.4 ± 0.3
3	31.2 ± 0.2	19.1 ± 0.3	22.0 ± 0.2	236.1 ± 0.3
4	10.2 ± 0.5	9.8 ± 0.2	12.0 ± 0.3	272.9 ± 0.4
5	22.9 ± 0.5	16.8 ± 0.2	21.9 ± 0.6	261.3 ± 0.9
6	15.4 ± 0.3	10.5 ± 0.1	18.4 ± 0.3	242.6 ± 0.2
7	17.2 ± 0.5	11.8 ± 0.2	18.5 ± 0.2	243.6 ± 0.3
8	9.4 ± 0.2	8.3 ± 0.4	10.9 ± 0.2	288.0 ± 0.5
Cisplatin	22.6 ± 0.8	14.9 ± 0.5	21.3 ± 0.9	221.3 ± 0.6

[a]IC_{50} = concentration of the drug required to inhibit growth of 50% of the cancer cells (μM).
The sign (>) indicates that IC_{50} value was not obtained up to given concentration.

2.5 Morphological changes in AO and EB dual staining

An Acridine Orange–Ethidium Bromide (AO–EB) dual fluorescent staining method was used to investigate apoptosis in a MDA-MB-231cell line treated with complex 4 and 8. After treatment of cells with the complexes 4 and 8 for 24 h and irradiated with visible light showed significant reddish-orange emission with condensed chromatin and membrane blebbing. In the control, the cells of MDA-MB-231 were stained bright green in spots. Henceforth, the morphological changes clearly indicate that the complexes induce cell death through apoptosis.

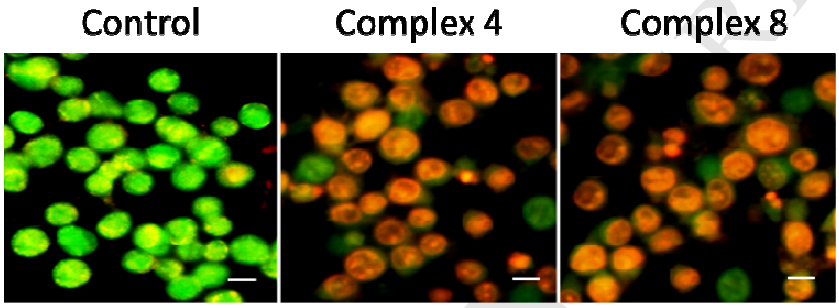

Fig. 3 Morphological assessment of AO and EB dual staining of MDA-MB-231cells treated with complex 4 & 8 (IC_{50} concentration) for 24 h. The scale bar 20 mm.

2.6 Morphological changes in Hoechst 33258 staining

To investigate the nuclear morphologic characteristics, MDA-MB-231 cells were stained with Hoechst 33258 and treated with complexes 4 and 8 using fluorescence microscopy. After 24 h, complexes treated cells showed fragmented nuclei and chromatin condensation which are features of apoptosis different from control cells (Fig.4).

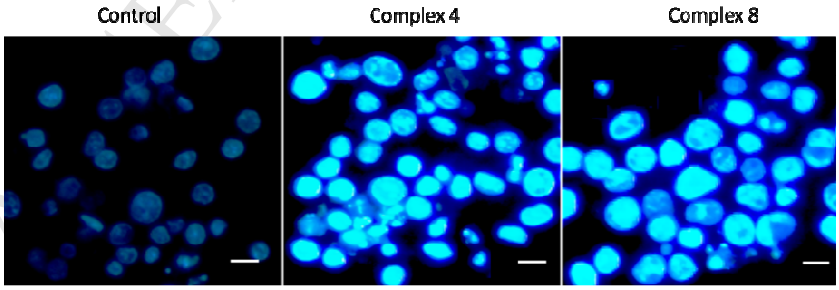

Fig. 4 Morphology of the nuclei of MDA-MB-231 cells observed by fluorescence microscopy (Hoechst 33258 staining, 24 h incubation at IC_{50} concentrations) after treatment with control complexes 4 and 8.

2.7 Evaluation of apoptosis – Flow cytometry

As shown in Fig. 5 and 6, MDA-MB-231cells were treated with complex 4 and 8 at two different concentrations for 24 h. The increase of annexin V+/PI+ (Q2) population from 3.7% to 6.7% for 4 and 5.0% to 8.2% for 8 at 50 and 100 µM concentrations of the complexes respectively represent cells undergoing apoptosis. Taken together, these results indicate that cell death induced by complexes is mainly caused by induction of apoptosis.

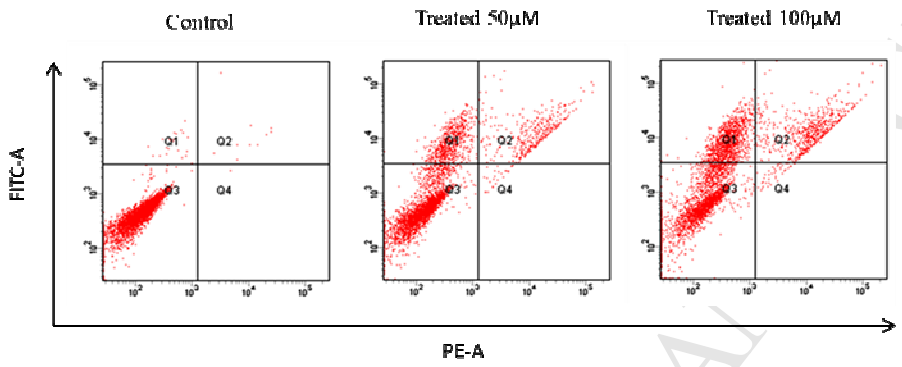

Fig. 5 Annexin V/propidium iodide assay of MDA-MB-231cells treated by complex 4 (50 and 100 µM concentration) measured by flow cytometry.

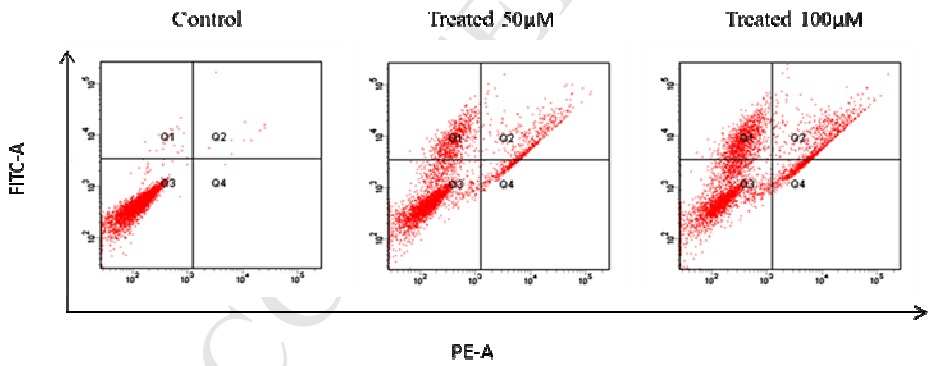

Fig. 6 Annexin V/propidium iodide assay of MDA-MB-231cells treated by complex 8 (50 and 100 µM concentration) measured by flow cytometry.

2.8 Comet assay

The comet assay was used to detect the DNA strand breaks with high sensitivity at the single-cell level [32]. As shown in Fig. 7, MDA-MB-231cells treated with IC_{50} concentration

of the complexes 4 and 8 for 24h show the increase in the length of the comet tail and illustrate that the complexes induce a remarkable DNA damage in a time-dependent manner, the percentage of DNA damage presented in Fig.S35 (ESI†). Further, the results of comet assay demonstrate that the complexes are capable of eliciting DNA damaging effects, as evidenced by the comet assays on MDA-MB-231 cells

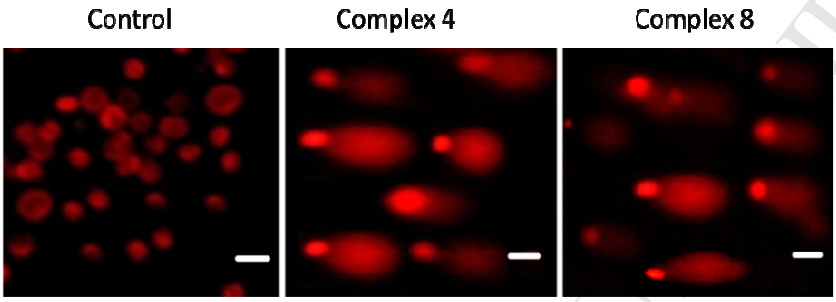

Fig. 7 Comet assay of EB-stained control, complex 4 and 8 treated breast cancer cells at 24h incubation.

3. Conclusions

In summary, we have described the synthesis of a series of arene ruthenium(II) benzhydrazone complexes. All the complexes have been completely characterized by analytical techniques and spectroscopic methods. Crystallographic studies of the complexes 6 and 7 have shown that the benzhydrazone ligands are coordinated to Ru(II) in a bidentate fashion via azomethine nitrogen and imidolate oxygen atoms. Besides, all the complexes were tested for anticancer activity against HeLa, MDA-MB-231, and Hep G2 cancer cell lines, and they were found to show excellent cytotoxicity to cancer cells without affecting the normal NIH 3T3 cells. Remarkably, complexes 4 and 8 display high cytotoxicity against cancer cell lines tested with very low IC_{50} values. Moreover, fluorescence staining techniques, flow cytometry and comet assays demonstrated that complexes induce apoptosis in MDA-MB-231 cells. Hence, confirming that these arene ruthenium(II) benzhydrazone complexes have promising biological properties and are worth investigating further.

4. Experimental

4.1 Reagents and materials

$RuCl_3.3H_2O$ was purchased from Loba Chemie Pvt. Ltd. and used as received. Aldehydes and benzhydrazide derivatives were obtained from Aldrich. All other chemicals

were purchased from commercial sources and used without further purification. The Solvents were distilled following the standard procedures [33] and degassed prior to use. [Ru(arene) (μ-Cl)Cl]$_2$ (arene= benzene and *p*-cymene) was prepared by reported procedure [34].

4.2 Physical measurements

FT-IR spectra in KBr pellets were recorded on a JASCO 400 plus spectrometer. Microanalysis of carbon, hydrogen, nitrogen and sulphur were carried out by Vario EL III CHNS elemental analyzer. UV- visible spectra was recorded on a CARY 300 Bio UV- Vis spectrometer. The ^{1}H NMR spectra were carried out with Bruker 400 MHz instruments. Melting points were determined on a Boetius micro-heating table and are corrected. ESI-MS spectra were obtained by micro mass Quattro II triple quadrupole mass spectrometer. The annexin V-FITC kit (APOAF-20TST) from Sigma-Aldrich was used based on manufacturer instructions.

4.3 Preparation of thiophene benzhydrazone ligands

A solution of thiophene-2-carboxyaldehyde (5 mmol) in ethanol (10mL) was added drop wise to the ethanol solution (10 mL) of 4-substituted benzhydrazide (5 mmol) and the reaction mixture was refluxed for about 3 h. The solution was concentrated to 5 ml and cooled to room temperature. The cream or pale brown solid formed was filtered, washed with cold methanol (5mL) and dried in air. Yield 83-88%.

4.4 Synthesis of arene ruthenium(II) benzhydrazone complexes

A mixture of [Ru (η^6-C_6H_6) (μ-Cl)Cl]$_2$ or [Ru (η^6-*p*-cymene) (μ-Cl)Cl]$_2$ (0.04 mmol) and benzhydrazone ligand (0.08 mmol) was refluxed in benzene in the presence of triethylamine (0.5 mL) for 5 h. After removing the triethylammonium chloride by filtration, the solution was concentrated and light petroleum ether (bp 60-80 ^{o}C) was added whereby the solid separated out. The resulted solids were recrystallized from CH_2Cl_2/petroleum ether and dried under vacuum.

4.4.1 [Ru(η^6-C_6H_6)(Cl)(L1)] (1). Colour: Brown; Yield: 80%; M.p.: 165 ^{0}C; Anal. Calc. For $C_{18}H_{15}ClN_2ORuS$: C, 48.70; H, 3.40; N, 6.31; S, 7.22%. Found: C, 48.52; H, 3.45; N, 6.30; S, 7.25%. IR (KBr, cm^{-1}):1598 $\nu_{(C=N-N=C)}$, 1265 $\nu_{(C-O)}$. UV–Vis (CH_3CN, λ max/nm;

ε/dm^3 mol^{-1} cm^{-1}): 354(3415), 274(4254), 236(6652). ^{1}H NMR (400 MHz, $CDCl_3$) (δ ppm): 8.9 (s, 1H, N=CH), 7.1–8.1 (m, 8H, aromatic), 5.5(s, 6H). ESI-MS (CH_3CN): calcd for $C_{18}H_{15}ClN_2ORuS$ m/z 443.96; found [M - Cl]$^+$:410.00.

4.4.2 [Ru(η^6-C_6H_6)(Cl)(L2)] (2). Colour: Brown; Yield: 77%; M.p.: 163 ^{0}C; Anal. Calc. For $C_{18}H_{14}Cl_2N_2ORuS$: C, 45.19; H, 2.94; N, 5.85; S, 6.70%. Found: C, 45.35; H, 2.90; N, 5.88; S, 6.72%. IR (KBr, cm^{-1}):1620 $\nu_{(C=N-N=C)}$, 1260 $\nu_{(C-O)}$. UV–Vis (CH_3CN, λ max/nm; ε/dm^3 mol^{-1} cm^{-1}): 366(1855), 281(2394), 238(4473). ^{1}H NMR (400 MHz, $CDCl_3$) (δ ppm): 8.9 (s, 1H, N=CH), 7.1–8.1 (m, 7H, aromatic), 5.5 (s, 6H). ESI-MS (CH_3CN): calcd for $C_{18}H_{14}Cl_2N_2ORuS$ m/z 477.92; found [M - Cl]$^+$:444.96.

4.4.3 [Ru(η^6-C_6H_6)(Cl)(L3)] (3). Colour: Brown; Yield: 74%; M.p.: 161 ^{0}C; Anal. Calc. For $C_{18}H_{14}BrClN_2ORuS$: C, 41.35; H, 2.69; N, 5.35; S, 6.13%. Found: C, 41.58; H, 2.67; N, 5.36; S, 6.19%. IR (KBr, cm^{-1}):1612 $\nu_{(C=N-N=C)}$, 1256 $\nu_{(C-O)}$. UV–Vis (CH_3CN, λ max/nm; ε/dm^3 mol^{-1} cm^{-1}): 361(7045), 273(8836), 244(12972). ^{1}H NMR (400 MHz, $CDCl_3$) (δ ppm): 8.9 (s, 1H, N=CH), 7.1–8.1 (m, 7H, aromatic), 5.5(s, 6H). ESI-MS (CH_3CN): calcd for $C_{18}H_{14}BrClN_2ORuS$ m/z 521.87; found [M - Cl]$^+$:486.89.

4.4.4 [Ru(η^6-C_6H_6)(Cl)(L4)] (4). Colour: Brown; Yield: 72%; M.p.: 157 ^{0}C; Anal. Calc. For $C_{19}H_{17}ClN_2O_2RuS$: C, 48.15; H, 3.61; N, 5.91; S, 6.76%. Found: C, 48.25; H, 3.67; N, 5.95; S, 6.71%. IR (KBr, cm^{-1}):1594 $\nu_{(C=N-N=C)}$, 1272 $\nu_{(C-O)}$. UV–Vis (CH_3CN, λ max/nm; ε/dm^3 mol^{-1} cm^{-1}): 360(5095), 279(5742), 253(7314). ^{1}H NMR (400 MHz, $CDCl_3$) (δ ppm): 8.9 (s, 1H, N=CH), 6.8–8.1 (m, 7H, aromatic), 5.5(s, 6H), 3.8 (s, 3H, OCH_3). ESI-MS (CH_3CN): calcd for $C_{19}H_{17}ClN_2O_2RuS$ m/z 473.97; found [M + H]$^+$:474.98, [M - Cl]$^+$:439.00.

4.4.5 [Ru(η^6-*p*-cymene)(Cl)(L1)] (5). Colour: Yellow; Yield: 85%; M.p.: 188 ^{0}C; Anal. Calc. For $C_{22}H_{23}ClN_2ORuS$: C, 52.84; H, 4.63; N, 5.60; S, 6.41%. Found: C, 52.67; H, 4.60; N, 5.64; S, 6.44%. IR (KBr, cm^{-1}):1596 $\nu_{(C=N-N=C)}$, 1259 $\nu_{(C-O)}$. UV–Vis (CH_3CN, λ max/nm; ε/dm^3 mol^{-1} cm^{-1}): 364(5516), 280(6007), 234(6622). ^{1}H NMR (400 MHz, $CDCl_3$) (δ ppm): 8.8 (s, 1H, N=CH), 7.1–8.0 (m, 8H, aromatic), 5.3 (d, *J* = 5.6 Hz, 1H, cymene Ar-H), 5.3 (d, *J* = 6 Hz, 1H, cymene Ar-H), 5.0 (d, *J* = 5.6 Hz, 1H, cymene Ar-H), 4.6 (d, *J* = 5.6 Hz, 1H, cymene Ar-H), 2.5 (m, 1H, CH of *p*-cymene), 2.2 (s, 3H, CH_3 of *p*-cymene), 1.0-

1.3 (dd, *J* = 94.8 Hz, *J* = 7.2 Hz, 6H, 2CH_3 of *p*-cymene). ESI-MS (CH_3CN): calcd for $C_{22}H_{23}ClN_2ORuS$ *m/z* 500.02; found $[M + H]^+$:501.03, $[M - Cl]^+$:465.05.

4.4.6 [Ru(η^6-*p*-cymene)(Cl)(L2)] (6). Colour: Yellow; Yield: 82%; M.p.: 180 ^{0}C; Anal. Calc. For $C_{22}H_{22}Cl_2N_2ORuS$: C, 49.43; H, 4.14; N, 5.24; S, 5.99%. Found: C, 49.28; H, 4.15; N, 5.22; S, 5.98%. IR (KBr, cm^{-1}):1599 $\nu_{(C=N-N=C)}$, 1262 $\nu_{(C-O)}$. UV–Vis (CH_3CN, λ max/nm; ε/dm^3 mol^{-1} cm^{-1}): 364(3579), 282(3771), 245(5264).^{1}H NMR (400 MHz, $CDCl_3$) (δ ppm): 8.8 (s, 1H, N=CH), 7.1–8.0 (m, 7H, aromatic), 5.3 (d, *J* = 6.4 Hz, 1H, cymene Ar-H), 5.3 (d, *J* = 6 Hz, 1H, cymene Ar-H), 5.0 (d, *J* = 5.6 Hz, 1H, cymene Ar-H), 4.6 (d, *J* = 5.6 Hz, 1H, cymene Ar-H), 2.5 (m, 1H, CH of *p*-cymene), 2.2 (s, 3H, CH_3 of *p*-cymene), 1.0-1.3 (dd, *J* = 100.8 Hz, *J* = 14.4 Hz, 6H, 2CH_3 of *p*-cymene). ESI-MS (CH_3CN): calcd for $C_{22}H_{22}Cl_2N_2ORuS$ *m/z* 533.98; found = $[M - Cl]^+$:499.02.

4.4.7 [Ru(η^6-*p*-cymene)(Cl)(L3)] (7). Colour: Yellow; Yield: 78%; M.p.: 178 ^{0}C; Anal. Calc. For $C_{22}H_{22}BrClN_2ORuS$: C, 45.64; H, 3.83; N, 4.83; S, 5.53%. Found: C, 45.43; H, 3.85; N, 4.81; S, 5.54%. IR (KBr, cm^{-1}):1607 $\nu_{(C=N-N=C)}$, 1260 $\nu_{(C-O)}$. UV–Vis (CH_3CN, λ max/nm; ε/dm^3 mol^{-1} cm^{-1}): 360(6761), 304(7395), 246(10158). ^{1}H NMR (400 MHz, $CDCl_3$) (δ ppm): 8.8 (s, 1H, N=CH), 7.1–8.0 (m, 7H, aromatic), 5.3 (d, *J* = 6 Hz, 1H, cymene Ar-H), 5.3 (d, *J* = 6 Hz, 1H, cymene Ar-H), 5.0 (d, *J* = 5.6 Hz, 1H, cymene Ar-H), 4.6 (d, *J* = 5.6 Hz, 1H, cymene Ar-H), 2.5 (m, 1H, CH of *p*-cymene), 2.2 (s, 3H, CH_3 of *p*-cymene), 1.0-1.3 (dd, *J* = 104 Hz, *J* = 7.2 Hz, 6H, 2CH_3 of *p*-cymene). ESI-MS (CH_3CN): calcd for $C_{22}H_{22}BrClN_2ORuS$ *m/z* 577.93; found $[M - Cl]^+$:544.96.

4.4.8 [Ru(η^6-*p*-cymene)(Cl)(L4)] (8). Colour: Yellow; Yield: 76%; M.p.: 168 ^{0}C; Anal. Calc. For $C_{23}H_{25}ClN_2O_2RuS$: C, 52.11; H, 4.75; N, 5.28; S, 6.04%. Found: C, 52.35; H, 4.70; N, 5.25; S, 6.08%. IR (KBr, cm^{-1}):1592 $\nu_{(C=N-N=C)}$, 1259 $\nu_{(C-O)}$. UV–Vis (CH_3CN, λ max/nm; ε/dm^3 mol^{-1} cm^{-1}): 361(4930), 291(5508), 246(7594). ^{1}H NMR (400 MHz, $CDCl_3$) (δ ppm): 8.8 (s, 1H, N=CH), 6.7–7.9 (m, 9H, aromatic), 5.3 (d, *J* = 6 Hz, 1H, cymene Ar-H), 5.3 (d, *J* = 6 Hz, 1H, cymene Ar-H), 5.0 (d, *J* = 5.6 Hz, 1H, cymene Ar-H), 4.6 (d, *J* = 5.6 Hz, 1H, cymene Ar-H), 3.7 (s, 3H, OCH_3), 2.5 (m, 1H, CH of *p*-cymene), 2.2 (s, 3H, CH_3 of *p*-cymene), 1.0-1.3 (dd, *J* = 101.6 Hz, *J* = 7.2 Hz, 6H, 2CH_3 of *p*-cymene). ESI-MS (CH_3CN): calcd for $C_{23}H_{25}ClN_2O_2RuS$ m/z 530.04; found $[M + H]^+$:531.04, $[M - Cl]^+$:495.06.

4.5 X-ray crystallography

A Single crystal of [Ru(η^6- *p*-cymene)Cl(L2)] **(6)** and [Ru(η^6- *p*-cymene)Cl(L3)] **(7)** were obtained Dichloromethane-Petroleum ether solution at room temperature by slow evaporation technique. X-Ray data were collected with a Bruker AXS Kappa APEX II single crystal X-ray diffractometer using monochromated Mo-Kα radiation (λ=0.71073). The structure solution was obtained by direct methods (SIR-97) [35] and refined using (SHELXL-97) full matrix least-squares calculations on F^2 [36]. All non-hydrogen atoms were refined anisotropically, hydrogen atoms were fixed geometrically and refined by riding model. The Bruker SAINT-Plus (Version 7.06a) software were used to analyse the Frame integration and data reduction. The multiscan absorption corrections were applied using SADABS software. CCDC reference number is 1449681-1449682**.**

4.6 Stability Studies

The stability of the complexes were carried out as described previously [37].

4.7 Partition Coefficient Determination

Partition coefficients (P) between n-octanol and water phases were carried out as described previously [27,38].

4.8 Cell culture

HeLa human cervical cancer cell line, MDA-MB-231 Triple negative breast carcinoma, Hep G2 human liver carcinoma cell line and NIH 3T3 noncancerous cell, mouse embryonic fibroblast were supplied by the National Centre for Cell Science (NCCS), Pune. The cell lines were cultured as a monolayer in RPMI-1640 medium (Biochrom AG, Berlin, Germany), supplemented with 10% fetal bovine serum (Sigma-Aldrich, St. Louis, MO, USA) and with 100 U mL^{-1} penicillin and 100 µg mL^{-1} streptomycin as antibiotics (Himedia, Mumbai, India), at 37 ^{o}C in a humidified atmosphere of 5% CO_2 in a CO_2 incubator (Heraeus, Hanau, Germany).

MTT assay, AO-EB staining, Hoechst 33258 staining, Flow cytometry and comet assay were evaluated as described previously [39-42].

Acknowledgments

One of the authors (N. M) thanks University Grants Commission (UGC), New Delhi, for the award of UGC-RFSMS. We express sincere thanks to DST-FIST, India for the use of

Bruker 400 MHz spectrometer at the School of Chemistry, Bharathidasan University, Tiruchirappalli. We thank Dr T. R. Santhosh Kumar for the flow cytometry analysis.

Appendix A. Supplementary material

^{1}H spectra of the complexes (1-8), The ESI-MS of the complexes (1-8) and log P Values for Complexes **1-8**. CCDC 1449681-1449682 contains the supplementary crystallographic data for this paper. These data can be obtained free of charge from The Cambridge Crystallographic Data Centre via www.ccdc.cam.ac.uk/data_request/cif.

References

[1] A. Bergamo, C. Gaiddon, J. H. M. Schellens, J. H. Beijnen, G. Sava, J. Inorg. Biochem. 106 (2012) 90-99.

[2] M. Groessl, C.G. Hartinger, K. Po1ec-Pawlak, M. Jarosz, P.J. Dyson, B.K. Keppler, Chem. Biodivers. 5 (2008) 1609-1614.

[3] C. G. Hartinger, P. J. Dyson, Chem. Soc. Rev., 38 (2009) 391–401.

[4] M. Hanif , S. M. Meier, W. Kandioller, A. Bytzek, M. Hejl, C. G. Hartinger, A. A. Nazarov, V. B. Arion, M. A. Jakupec, P. J. Dyson, B. K. Keppler, J. Inorg. Biochem. 105 (2011) 224–231

[5] S. M. Meier, M. Hanif, W. Kandioller, B. K. Keppler, C. G. Hartinger, J. Inorg. Biochem. 108 (2012) 91–95

[6] A. Egger, V. B. Arion, E. Reisner, B. Cebri´an-Losantos, S. Shova, G. Trettenhahn, B. K. Keppler, Inorg. Chem., 44 (2005) 122-132.

[7] Claudine Scolaro, A. B. Chaplin, C. G. Hartinger, A. Bergamo, M. Cocchietto, B. K. Keppler, G. Sava P. J. Dyson, Dalton Trans., (2007) 5065–5072.

[8] G. Süss-Fink, Dalton Trans. 39 (2010) 1673-1688.

[9] W. Kandioller, C. G. Hartinger, A. A. Nazarov, J. Kasser, R. John, M. A. Jakupec, V. B. Arion, P. J. Dyson, B. K. Keppler, J. Organomet. Chem., 694 (2009) 922-929.

[10] C. G. Hartinger, N. Metzler-Nolte, P. J. Dyson, Organometallics 31 (2012) 5677-5685.

[11] G. S. Smith, B. Therrien, Dalton Trans. 40 (2011) 10793-10800.

[12] L. D. Dale, J. H. Tocher, T. M. Dyson, D. I. Edwards, D. A. Tocher, Anti-cancer Drug Des., 7 (1992) 3-14.

[13] C.S. Allardyce, P.J. Dyson, D.J. Ellis, S.L. Heath, Chem. Commun. (2001) 1396-1397.

[14] R.E. Morris, R.E. Aird, P.d.S. Murdoch, H. Chen, J. Cummings, N.D. Hughes, S. Pearsons, A. Parkin, G. Boyd, D.I. Jodrell, P.J. Sadler, J. Med. Chem. 44 (2001) 3616-3621.

[15] P. Govender, B. Therrien, G.S. Smith, Eur. J. Inorg. Chem. (2012) 2853-2862.

[16] V. Onnis, M. T. Cocco, R. Fadda, C. Congiu, Bioorg. Med. Chem., 17 (2009) 6158-6165.

[17] M.R. Maurya, S. Agarwal, M. Abid, A. Azam, C. Bader, M. Ebel, D. Rehder, Dalton Trans. (2006) 937-947.

[18] D.K. Johnson, T.B. Murphy, N.J. Rose, W.H. Goodwin, L. Pickart, Inorg. Chim. Acta 67 (1982) 159-165.

[19] T.B. Chaston, D.B. Lovejoy, R.N. Watts, D.R. Richardson, Clin. Cancer Res. 9 (2003) 402-414.

[20] E. Jayanthi, S. Kalaiselvi, V. Vijaya Padma, N. S.P. Bhuvanesh, N. Dharmaraj, Inorg. Chim. Acta 429 (2015) 148-159.

[21] K. K. Upadhyay, A. Kumar, R. K. Mishra, T. M. Fyles, S. Upadhyaya, K. Thapliyalc, New. J. Chem. 34 (2010) 1862-1866.

[22] R. Raveendran, S. Pal, J. Organomet. Chem., 692 (2007) 824-830.

[23] (a) S. N. Pal, S. Pal, J. Chem. Soc., Dalton Trans., (2002) 2102-2108; (b) R. Raveendran, S. Pal, Polyhedron, 24 (2005) 57-63.

[24] F.A. Beckford, G. Leblanc, J. Thessing, M. Shaloski Jr., B.J. Frost, L. Li, N.P. Seeram, Inorg. Chem. Commun. 12 (2009) 1094–1098.

[25] (a) R. K. Gupta, R. Pandey, G. Sharma, R. Prasad, B. Koch, S. Srikrishna, P.-Z. Li, Q. Xu, D. S. Pandey, Inorg. Chem., 52 (2013) 3687–3698. (b) H. Huang, P. Zhang, Y. Chen, K. Qiu, C. Jin, L. Ji, H. Chao, Dalton Trans., 45 (2016) 13135.

[26] J. D. Aguirre, A. M. Angeles-Boza, A. Chouai, Jean-Philippe Pellois, C. Turro, K. R. Dunbar, J. Am. Chem. Soc. 131 (2009) 11353-11360.

[27] R. K. Gupta, R. Pandey, G. Sharma, R. Prasad, B. Koch, S. Srikrishna, P.-Z. Li, Q. Xu and D. S. Pandey, Inorg. Chem., 52 (2013) 3687-3698.

[28] (a) R. Pignatello, T. Musumeci, L. Basile, C. Carbone, G. Puglisi, J. Pharm. Bioallied Sci. 3 (2011) 4-14. (b) M. Fresta, S. Guccione, A. R. Beccari, P. M. Furneric, G. Puglisi, Bioorg. Med. Chem. 10 (2002) 3871-3889.

[29] S. Mukhopadhyay, R. K. Gupta, R. P. Paitandi, N. K. Rana, G. Sharma, B. Koch, L. K. Rana, M. S. Hundal and D. S. Pandey, Organometallics, 2015, 34, 4491–4506.

[30] F. Caruso, R. Pettinari, M. Rossi, E. Monti, M. B. Gariboldi, F. Marchetti, C. Pettinari, A. Caruso, M. V. Ramani, G. V. Subbaraju, J. Inorg. Biochem. 162 (2016) 44 -51.

[31] (a)G. Lv, L. Guo, L. Qiu, H. Yang, T. Wang, H. Liu, J. Lin, Dalton Trans., 44 (2015) 7324–7331. (b) H. Lai, Z. Zhao, L. Li, W. Zheng, T. Chen, Metallomics, 7 (2015) 439-447. (c) H. Sabine, V. Rijt, A. Mukherjee, A. M. Pizarro, P. J. Sadler, J. Med. Chem. 2010, 53, 840–849. (d) M. Ganeshpandian, M. Palaniandavar, A, Muruganantham, S. K. Ghosh, A. Riyasdeen, M. A. Akbarsha, App. Organometal Chem. 2017;e4154. (f) M. R. Gill, J. A. Thomas, Chem. Soc. Rev., 41 (2012) 3179–3192.

[32] A. Hartmann, G. Speit, Mutat. Res., 346 (1995) 49-56.

[33] W.L.F. Armarego, C.L.L. Chai, Purification of Laboratory Chemicals, sixth ed. Butterworth-Heinemann, Oxford, UK, 2009 pp 69-79.

[34] M.A. Bennett, A.K. Smith, J. Chem. Soc. Dalton Trans. (1974) 233-241.

[35] F.H. Allen, W.D.S. Motherwell, P.R. Raithby, G.P. Shields, R. Taylor, New. J. Chem. 23 (1999) 25-34.

[36] G.M. Sheldrick, Acta Crystallogr. Sect. A. 64 (2008) 112-122.

[37] M. Mohamed Subarkhan, R. Ramesh, Yu Liu New J. Chem. 40 (2016) 9813–9823.

[38] R. Raj Kumar, R. Ramesh, J.G. Małecki J. Photochemi & Photobiology, B: Biology, 165 (2016) 310–327.

[39] M. Mohamed Subarkhan, R. Ramesh, Inorg. Chem. Front. 3 (2016) 1245-1255.

[40] (a) M. Blagosklonny and W. S. El-Diery, Int. J. Cancer, 67 (1996) 386–392. (b) R. Raj Kumar, R. Ramesh, J.G. Małecki, New J. Chem. 41 (2017) 9130–9141.

[41] G. P. A. H. Kasibhatla, D. Finucane, T. Brunner, E. B. Wetzel and D. R. Green, Protocol: Staining of suspension cells with Hoechst 33258 to detect apoptosis, in Cell: A laboratory manual Culture and Biochemical Analysis of Cells, CSHL Press, USA, 1998, vol. 1, p. 15.5.

[42] C. R. Sihn, E. J. Suh, K. H. Lee, T. Y. Kim and S. H. Kim, Cancer Lett., 201 (2003) 203–210.

- Synthesis and characterization of arene ruthenium(II) benzhydrazone complexes.
- The single-crystal X-ray structure analysis of two complexes is depicted.
- The complexes have been screened for their *in vitro* antiproliferative activities.
- The mechanism of action of the most potent complexes was evaluated.